Target-current spectroscopy of reconstructing 5*d*-transition-metal surfaces as a tool for testing bulk-band-structure calculations

R. Drube
Max-Planck-Institut für Plasmaphysik, Boltzmannstrasse 2, D-W-8046 Garching bei München, Federal Republic of Germany

J. Noffke
Technische Universität Clausthal, Leibnizstrasse 10, D-W-3392 Clausthal-Zellerfeld, Federal Republic of Germany

R. Schneider
Max-Planck-Institut für Plasmaphysik, Boltzmannstrasse 2, D-W-8046 Garching bei München, Federal Republic of Germany

J. Rogozik
Elektronik System Gesellschaft, Vogelweideplatz 9, D-W-8000 München 80, Federal Republic of Germany

V. Dose
Max-Planck-Institut für Plasmaphysik, Boltzmannstrasse 2, D-W-8046 Garching bei München, Federal Republic of Germany
(Received 19 June 1990; revised manuscript received 3 July 1991)

Experimental target-current-spectroscopy (TCS) data of iridium and platinum are presented for the unreconstructed and the reconstructed (100) surface modifications. The effects of reconstruction on the coupling of free electrons to bulk bands are discussed with reference to a fully relativistic bulk-band-structure calculation. A TCS-based method for absolute work-function determinations is presented. For the unreconstructed (100) surfaces of iridium and platinum we obtain $\Phi_1=6.1\pm0.1$ eV and $\Phi_2=5.5\pm0.2$ eV, respectively. Reconstruction-induced changes of the work function amount to -0.1 eV for platinum and -0.2 eV for iridium.

INTRODUCTION

One of the best known surface analytical techniques is low-energy electron diffraction (LEED). The typical energies employed in this method range from 30 to 300 eV. Inelastically scattered electrons are removed from the total scattered flux by retarding fields acting as a high pass filter. The transmitted elastically diffracted electrons reveal the surface periodicity. The energy dependence of a single LEED spot [in the limit of very low energies also named very-low-energy electron diffraction (VLEED)] is frequently used to get information about the surface relaxation and surface reconstruction models. The LEED intensity analysis calculates intensity versus energy spectra for different geometrical models and compares these trial results with experimentally recorded data. This process is iterated until a best fit in the sense of a minimum R factor is obtained.[1] For this analysis an energy- and momentum-dependent calculation for the electron reflectivity of the surface must be carried out.[2,3] Due to the small probing depth, VLEED responds sensitively to changes in the surface barrier,[4] especially for kinetic energies of only a few eV.[5] A comparison of experimentally observed variations in the diffracted and the transmitted current with critical-point energies of the bulk-band structure was proposed by Jaclevic and Davis.[6] Since the latter method is the simpler one to measure the surface reflectivity, the target-current spectroscopy (TCS) is used in this work. The total sample current, i.e., the electron transmission T, is measured as a function of the energy of the incoming electrons. The inelastic part $R_{\rm in}$ varies only slowly with the electron energy.[7] The secondary-electron-emission current has larger variations only over a range of about 10 eV.[8–11] The dependence of the secondary-electron emission is shown in the discussion of Fig. 1 as follows. All distinct and sharp structures in the target current are an effect of those electrons that have been reflected elastically. This elastic part $R_{\rm el}$ is calculated by LEED theory and observed by VLEED measurements. The transmission T depends on the reflectivity

$$T=1-R_{\rm el}-R_{\rm in}\ . \tag{1}$$

For energies where only the (0,0) beam is visible TCS data contain the same information as VLEED data due to the weak variation of $R_{\rm in}$.

EXPERIMENTAL SETUP

The equipment used to measure TCS data is shown in the inset of Fig. 1. TCS needs an electron gun with a current-voltage characteristic which is only weakly energy dependent and produces no structure in the spectra.[12] Our electron gun is of a single-lens type and contains a BaO cathode. To determine changes in the work function Φ_P of the inspected surface the gun must not run in space-charge operation mode. At an emission current of

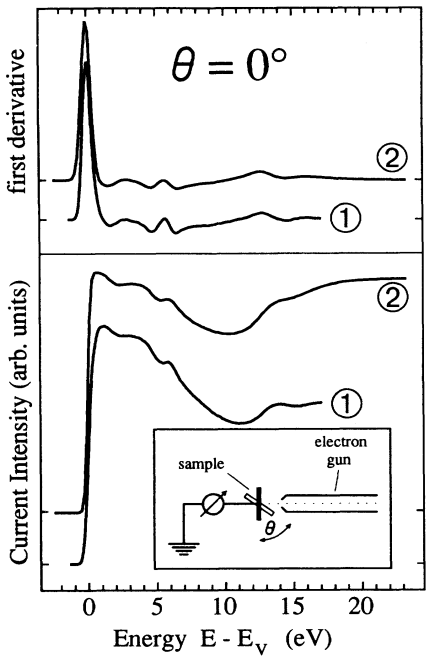

FIG. 1. Comparison of TCS data measured at normal incidence. Spectrum 1 is recorded with sample potential held on ground. Spectrum 2 is measured by variation of the sample potential. The upper panel shows the first derivatives of 1 and 2 as explained in the text. In the inset we show a schematic of the experimental equipment used in this work. The sample can be rotated relative to the electron gun to vary the angle of incidence θ of the electrons.

1 μA an extraction voltage of 150 V was sufficient to obtain saturation. In addition, the cathode must be burned in for many days to prevent work-function shifts, $\Delta\Phi_C$, of the work function Φ_C of the cathode and concomitant energy shifts of the measured TCS spectra. The gun is of similar type to that mentioned in Ref. 13. For this gun the energy resolution was determined to $\sigma^2_{\text{gun}}=(129\ \text{meV})^2$. The beam spot on the sample has a constant diameter of about 1 mm for acceleration voltages between 2 and 30 eV. The target current is measured as a function of the kinetic energy of the incoming electrons:

$$E_{\text{kin}}=e\Phi_C+eU-e\Phi_P\ . \tag{2}$$

U is the potential difference between cathode and sample. The momentum of the electrons parallel to the surface $\mathbf{k}_\parallel$ can be changed by rotating the sample through an angle θ relative to the electron gun:

$$\mathbf{k}_\parallel=[(2m_e/\hbar^2)E_{\text{kin}}]^{1/2}\sin\theta\ . \tag{3}$$

To record $\mathbf{k}_\parallel$-dependent, that is, off-normal, TCS data the region between sample and electron gun must be free of electric and magnetic fields which can be checked by TCS itself.[14] So any magnetic parts of the gun must be avoided. The field-free region also requires compensation for the work-function difference of the sample, the vacuum vessel, and the last lens element of the gun. In practice it is often sufficient to keep the sample and lens exit at ground potential. The electron energy is in both cases adjusted by variation of the cathode potential with respect to ground.

To verify suitability, the electron gun can be checked for normally incident electrons by comparing two different operating modes. The first mode is to ground the sample and vary the cathode potential. In the second mode we measure at constant cathode potential and apply a variable acceleration potential onto the sample. In this way the current-voltage characteristic of the gun does not disturb the spectra because the gun conditions are kept constant. A comparison of results from these two operation modes is shown in Fig. 1. Due to secondary-electron emission the total current as a function of energy becomes progressively smaller. Despite showing differences between the two operation modes we emphasize that the sharp fine structure in both data sets is the same. If we examine the maxima and minima of the first derivative of our spectra shown in the upper part of Fig. 1, we see that the onsets of the spectra lie accurately at the same energy position. The first maximum in the current at about 1 eV above the vacuum level is influenced by the gun characteristic but not the maximum in the first derivative. We therefore can take this maximum to detect shifts of the work function with a very high accuracy. As can also be seen in Fig. 1, the change in the operation mode and, therefore, the gun characteristic causes energy shifts of the maxima in the first derivative of about 0.15 eV up to 6 eV above vacuum level. This leads to uncertainties of absolute energy positions, but the determination of the absolute work function and work-function shifts does not need the absolute energy values. On the other hand, it is necessary to run the gun in a constant operation mode to reproduce the TCS data very well and with a high signal-to-noise ratio to avoid disturbing effects in the first derivative. In fact, we will mainly deal with the energy derivative of TCS spectra in later parts of this paper. So we conclude that the electron gun employed in this work performs satisfactorily for TCS measurements.

We wish to note that the TCS technique presented in this work is an ideal extension of inverse photoemission (IPE). All the experimental setup is already available and the information from TCS deals especially with initial-state coupling in IPE. Using sophisticated methods described in this work, sometimes it is also possible to extract absolute work functions from TCS data in addition to traditional techniques.[15]

THEORETICAL DESCRIPTION

In this work we try to describe the major features of observed TCS data by use of fully relativistic bulk-band structures, which were obtained by means of the linear rigorous cellular (LRC) method.[16,17] For computational reasons the excited bands have been calculated with the linear-augmented-plane-wave method using the self-consistent LRC potential. This leads to an uncertainty of at most 0.2 eV for the band energies with respect to very accurate LRC calculations. At a given energy a small reflection coefficient (i.e., a high transmission coefficient) can be expected if a large number of bulk states is avail-

able. The number of all bulk states for a defined $\mathbf{k}_{\parallel}$ within a mirror plane is something like the integration of the bulk-band structure over the one dimension of $\mathbf{k}_{\perp}$. This makes a projection of every state on $\mathbf{k}_{\parallel}$. Consequently we expect this projected $\mathbf{k}_{\parallel}$-dependent density of states (DOS) for the mirror plane under investigation to provide a guideline to the energy-dependent reflection (transmission) of an incident electron beam. However, only free-electron-like states with correct group velocities will contribute to the transmission coefficient.[12,18] We therefore try to introduce a quantitative criterion to determine to what extend a state is free-electron-like. That means we must calculate a "nearly-free-electron density of states" (NFE-DOS). A handwaving definition of this term is presented in the following. In the vacuum region the impinging electrons have $E_{\text{vacuum,free}}(\mathbf{k})$. Upon traversing the surface the electrons are accelerated normal to the surface by the inner potential V_0. In addition, the exchange of reciprocal-lattice vectors $\mathbf{G}$ with the crystal becomes possible. Energy conservation dictates

$$E_{\text{vacuum,free}}(\mathbf{k}) = E_{\text{crystal,free}}(\mathbf{k},\mathbf{G}) = (\hbar^2/2m_e)(\mathbf{k}-\mathbf{G})^2 - V_0 \ . \quad (4)$$

We now correlate the free-electron bands lowered by V_0 with the bulk bands. The unknown inner potential V_0 is adjusted such that the modified free-electron bands $E_{\text{crystal,free}}(\mathbf{k},\mathbf{G})$ exhibit maximum overlap with the calculated bulk-band structure in the energy range of 10–20 eV above Fermi level. The shaded bands in Fig. 2 result from a choice of $V_0 = -2 \pm 0.3$ eV for both samples. The complete free-electron band structure can be calculated by combining all possible reciprocal-lattice vectors $\mathbf{G}$ with the momentum $\mathbf{k}$ in Eq. (4).

To calculate the NFE-DOS, the energy scale was divided up into intervals of 0.1 eV. The theoretical three-dimensional bulk band structure was available for energies up to 45 eV above the valence-band minimum on a grid of 349 $\mathbf{k}$ points in $\frac{1}{48}$ of the bulk Brillouin zone. In addition, the angular-momentum projections were given up to $L = 3$. With the help of this information the energy eigenvalues were grouped into energy bands as a function of $\mathbf{k}$, $E_{\text{theory}}(\mathbf{k},n)$. By scanning the whole $\mathbf{k}$ region of the selected mirror plane and over all energy bands, we count the states falling within our energy windows. The procedure requires a three-dimensional interpolation algorithm to get $E(\mathbf{k})$ values at any arbitrary value of $\mathbf{k}$. Empirically, a simple mathematical polynomial interpolation algorithm of order 3 in every component of $\mathbf{k}$ and all mixed terms leads to satisfactory results. This algorithm makes use of 20 neighboring $\mathbf{k}$ points and reproduces the original values at every $\mathbf{k}$ point. On the boundary which may be accessed from two different central $\mathbf{k}$ points the respective interpolated energies differ by at most 20 meV.

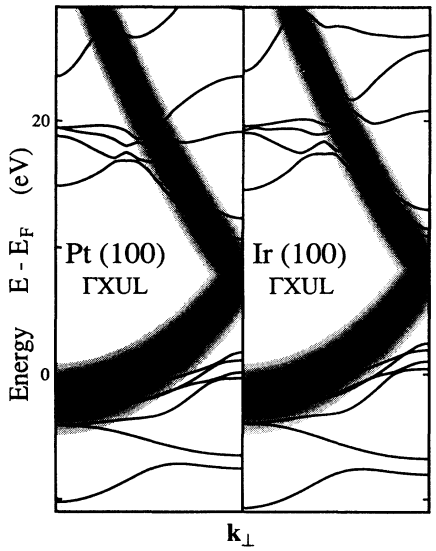

FIG. 2. Comparison of the bulk band structure of iridium and platinum for normal electron incidence with the free-electron parabola lowered by the inner potential of 2 eV. The broadening of the parabola shall quantify the lifetime broadening of the excited states and shows the range of acceptance for free-electron-like bulk bands.

To quantify the comparison between bulk band structure and free-electron band structure the states are weighted before counting for the NFE-DOS. An intuitive measure makes use of the energy-versus-momentum relation only. We have weighted our states as described in the following. First we have to check the similarity of the energies. For an ideal free-electron-like bulk band the energy difference ΔE between the free-electron-like energy $E_{\text{crystal,free}}(\mathbf{k},\mathbf{G})$ and the calculated bulk band energy of the nth band $E_{\text{theory}}(\mathbf{k},n)$ must vanish:

$$\Delta E = E_{\text{crystal,free}}(\mathbf{k},\mathbf{G}) - E_{\text{theory}}(\mathbf{k},n) \ . \quad (5)$$

The degree to which (5) is satisfied for a particular band is expressed in terms of a Gaussian $g_1(\Delta E,\sigma_\tau)$ with

$$g_1 = \exp[-0.5(\Delta E/\sigma_\tau)^2] \ , \quad (6)$$

with

$$\sigma_\tau = 0.1\{7 + [(E_{\text{theory}} - E_F)/(1\text{ eV})]^{1/2}\}\text{ eV} \ . \quad (7)$$

The above definition of σ_τ results in a variance of about 1 eV at an energy of $(E_{\text{theory}} - E_F) = 10$ eV. The energy dependence of σ_τ will quantify the lifetime broadening of the excited energy bands. Its functional form has been chosen on the basis of previous experience with LEED.[19] An alternative linearly energy-dependent linewidth has been postulated by Altmann[20] on the basis of line-shape analysis of inverse photoemission and photoemission data. The difference is unimportant for the present application. Figure 2 shows the bulk band structure for the (100) surfaces of iridium and platinum for normal incidence as solid black lines. The free-electron parabola is drawn with the energy range of g_1 by different gray scalings.

We next compare the dispersion of the bands $E_{\text{theory}}(\mathbf{k},n)$ and $E_{\text{crystal,free}}(\mathbf{k},\mathbf{G})$. As mentioned before, the coupling of the free-electron bands to the bulk states should have an optimum if the associated group velocities match. We quantify this requirement by

$$\Delta E_{\mathbf{k}} = \Delta(\partial E/\partial\mathbf{k}) = [\partial E_{\text{crystal,free}}(\mathbf{k},\mathbf{G})/\partial\mathbf{k}] - [\partial E_{\text{theory}}(\mathbf{k},n)/\partial\mathbf{k}] \ . \quad (8)$$

The degree to which (8) is satisfied for a particular band is expressed in terms of a Gaussian $g_2(\Delta E_{\mathbf{k}},\sigma_{\mathbf{k}})$ with

$$g_2=\exp[-0.5(\Delta E_{\mathbf{k}}/\sigma_{\mathbf{k}})^2] . \tag{9}$$

A choice of

$$\sigma_{\mathbf{k}}=15\ \text{eV}\,\text{Å}^{-1} \tag{10}$$

is consistent with the above choice of ΔE on the basis of free-electron dispersion at $(E_{\text{theory}}-E_F)=15$ eV. The energy dependence of $\sigma_{\mathbf{k}}$ has been neglected. From g_1 and g_2 we form the weighting factor $g=g_1g_2$. The pictures shown in the following part of this work symbolize the two-dimensional NFE-DOS $(E,\mathbf{k}_{\parallel})$ by a linear gray step grid. White areas indicate no available state and include the relative bulk band gaps.

For the weighting of the NFE states only those reciprocal lattice vectors should be considered that lie in the inspected mirror plane. In Fig. 3 the smallest reciprocal lattice vectors except $\langle 000\rangle$ that lie within the two mirror planes ΓXUL and ΓXWK of a (100) surface are shown. For the (100) surface in the ΓXWK azimuth only the vectors $\langle 200\rangle$, $\langle 020\rangle$, and $\langle 0\bar{2}0\rangle$ must be considered. The contributions of the different vectors depend on the angle θ of the incoming electrons: the contributions of the $\langle 200\rangle$ scale with $\cos(\theta)$, the contribution of $\langle 020\rangle$and $\langle 0\bar{2}0\rangle$ scales with $\sin(\theta)$. For the ΓXUL azimuth of the (100) surface the θ-dependent decomposition into $\langle 200\rangle$, $\langle 111\rangle$, $\langle \bar{1}11\rangle$, $\langle 1\bar{1}\bar{1}\rangle$, and $\langle \bar{1}\bar{1}\bar{1}\rangle$ can be done as follows: Only the $\langle 111\rangle$-like vectors contribute to the parallel momentum $\mathbf{k}_{\parallel}$. To be consistent with the notation of the surfaces and the different directions we denote our vectors in the form $\langle \mathbf{k}_z,\mathbf{k}_y,\mathbf{k}_x\rangle$. Since $\mathbf{k}_x$ must be equal to $\mathbf{k}_y$ in the ΓXUL azimuth, an arbitrary vector $\langle \mathbf{k}_z,\mathbf{k}_x,\mathbf{k}_x\rangle$ determines by the sign of $\mathbf{k}_x$ whether the vectors $\langle 111\rangle$, $\langle \bar{1}11\rangle$ or $\langle 1\bar{1}\bar{1}\rangle$, $\langle \bar{1}\bar{1}\bar{1}\rangle$ must be considered. On the other hand if $|\mathbf{k}_z|$ is greater than $|\mathbf{k}_x|$, then the vector $\langle 111\rangle$ is the correct one. With these two conditions the decomposition can be done uniquely. The decomposition into the different lattice vectors $\mathbf{G}$ has the consequence that the zone boundaries are no longer symmetry points of the NFE-DOS. Only the qualitative symmetry like absolute bulk gaps is conserved.

Our calculation will be compared in the next section with first-derivative TCS spectra. The first derivative is calculated by convoluting the unsmoothed data with a differentiated Gaussian with a variance of $(0.4\ \text{eV})^2$ (Ref. 21) which simultaneously filters out statistical noise in the raw data. The value of 0.4 eV is small compared to the experimental resolution of about 0.7 eV or the full width at half maximum of 1.6 eV which can be seen at the onset region of the TCS data at vacuum level. With experimental resolution here we denote the minimum energetic difference of two structures to identify them as two and not as one structure. This is the error of the determination of an absolute energy position of a band-gap edge or another TCS structure. However, to get the absolute value of the work function from the symmetry method described later, it is only necessary that the TCS spectra can be reproduced with a very high precision. So the gun must run in a very constant operation mode, all spectra must be recorded within a short time period to void contamination of the sample, and the signal-to-noise ratio must be very large. Finally, the determination of the work-function shift upon reconstruction of the sample is the most exact method: With the previously mentioned high signal-to-noise ratio you only have to measure TCS from the unreconstructed phase, heat up the sample to induce reconstruction, and do a second TCS run with exactly the same operating conditions of the gun. In this way the shift of the focal point at the onset of the TCS spectra can be resolved up to 0.05 eV. If structures like upper- and lower-gap boundaries in the NFE-DOS have a steplike behavior as a function of energy, then maxima and minima in the first derivative of the TCS data will signal them experimentally at the correct energy position. Indeed, the finite experimental resolution only smears out the step but the energy position of its maximal first derivative will remain unchanged. If the behavior of the structures is peaklike, our interpretation of the TCS data will result in energetically shifted gap edges of 0.6 eV at most. This shift is downward for the upper-gap edge and upward for the lower-gap edge, i.e., we obtain an apparent gap narrowing. From the kinetic energy E_{kin} and the angle of incidence θ the parallel momentum $\mathbf{k}_{\parallel}$ can be calculated as shown in Eq. (3).

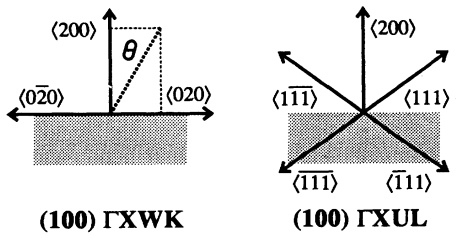

FIG. 3. The smallest reciprocal-lattice vectors of the (100) surface in the ΓXUL and the ΓXWK azimuth. The gray box symbolizes the bulk region.

EXPERIMENTAL DATA AND DISCUSSION

The (100) surface of iridium can be prepared in two modifications, a metastable unreconstructed (1×1) and a reconstructed (1×5) phase.[22] The reconstructed first monolayer has a nearly perfect hexagonal symmetry.[23] The preparation was done by absorbing NO at room temperature and reacting off the oxygen with hydrogen at about 430 K, according to Ref. 24. The sample condition was monitored by LEED and Auger spectroscopy. During the measurements the sample was held at room temperature. We present TCS data from the reconstructed and unreconstructed modification for different angles of electron incidence θ. The upper left panel in Fig. 4 shows the target current spectra of the unreconstructed (1×1) surface modification of Ir(100) in the ΓXUL azimuth as a function of $E_{\text{kin}}=E-E_V$ where E_V denotes the vacuum level. The first derivative of these data is calculated as described above and shown in the lower left panel of Fig. 4. The right part of Fig. 4 displays spectra for the reconstructed (1×5) phase and their first derivatives. The vac-

uum level of the unreconstructed (1×1) phase is taken from Ref. 25 to $\Phi_{Ir}^{1\times1}=6.1$ eV. An independent determination of this value is presented later in this work. The shift in the work function by changing the surface phase from (1×1) to (1×5) upon heating up the sample can be seen by a shift of the onset of two TCS spectra recorded subsequently, the first with the unreconstructed surface phase, the second with the reconstructed phase. This shift was measured to 0.2±0.05 eV. This compares favorably with previous measurements of 0.15 eV (Refs. 25 and 26) and 0.1 eV (Ref. 24). Together with the already quoted data of Wandelt, $\Phi_{Ir}^{1\times1}=6.1$ eV, we determine an absolute work function for Ir(100)-(1×5) of $\Phi_{Ir}^{1\times5}=5.9$ eV. Maxima and minima in the first derivative of our TCS data in Fig. 4 are plotted together with the NFE-DOS $(E,\mathbf{k}_{\parallel})$ in Fig. 5 for both ΓXUL and ΓXWK azimuth. For TCS data from the reconstructed (1×1) phase, maxima in the first derivative are symbolized by bold pluses, minima by solid triangles. Similar symbols (pluses and open triangles) denote maxima and minima in the first derivative of the TCS data on the reconstructed (1×5) phase. The size of the symbols is taken as a qualitative measure of how prominently the respective structure shows up in the TCS derivative spectra. Unfortunately, in some parts of the figure both types of symbols overlap. Special mention will be made in the text whenever necessary.

We shall now discuss a comparison of experiment and NFE-DOS calculation for the unreconstructed (1×1) surface of Ir(100). The experimentally detected upper edge of the bulk gap that starts at the $\bar{\Gamma}$ point at 11 eV and disperses downward is reproduced well by the theory. The gap at $\bar{X}$ at 13 eV is predicted at energies shifted 0.8 eV to higher values than observed by experiment. Semiempirical shifts of a band structure can be found, for example, in the work of Leschik *et al.*,[17] Courths *et al.*,[27] and Müller *et al.*[28] to fit experimental data even in a quantitative way to theoretical calculations. The gap seen at 17 eV around $\bar{X}$ is reproduced nearly perfectly by the theory. Only the lower boundary seems to disperse a little bit weaker with $\mathbf{k}_{\parallel}$ than predicted. The gap at 20 eV at $\bar{X}$ is also reproduced well at its lower boundary by theory. At the upper boundary the theory predicts current structures on the other side of $\bar{X}$ that cannot be

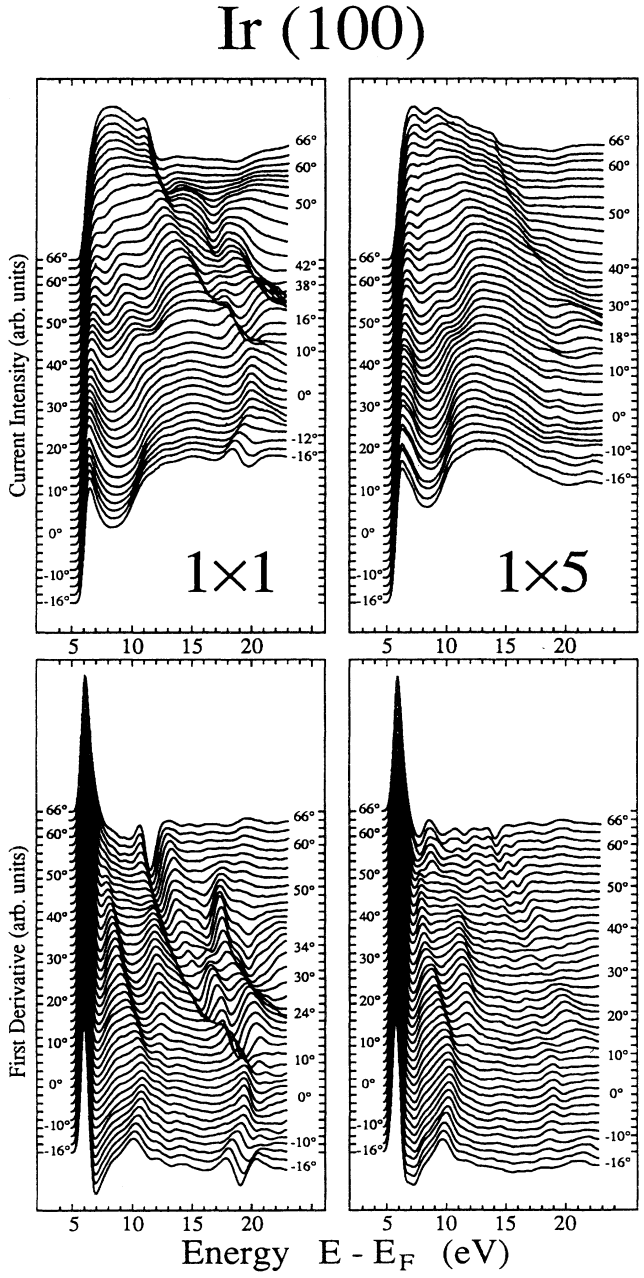

FIG. 4. Target current spectra from the unreconstructed 1×1 and the reconstructed 1×5 surface modification of Ir(100) in the ΓXUL azimuth. For both modifications the original data and their first derivatives are presented.

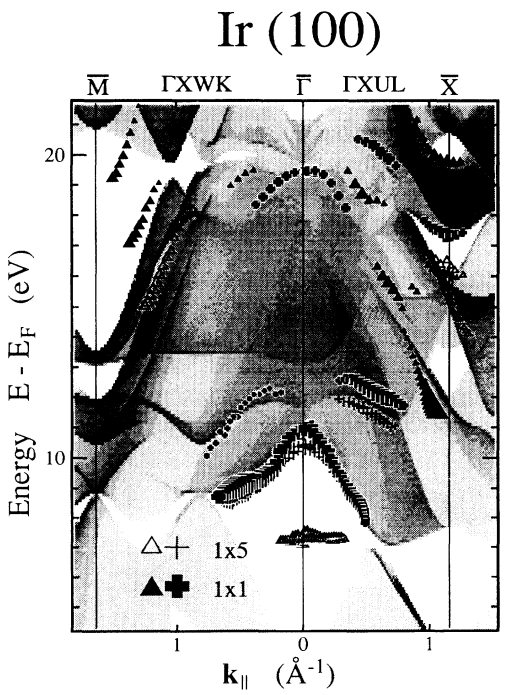

FIG. 5. Maxima and minima of the first derivative TCS data from Ir(100) in the ΓXUL (right part) and the ΓXWK azimuth (left part) as a function of $\mathbf{k}_{\parallel}$. With a linear gray scaling the NFE-DOS $(E,\mathbf{k}_{\parallel})$ of the surfaces are symbolized.

observed in the experiment. The narrow gap at $\bar{\Gamma}$ around 21.5 eV lies within a region of only small NFE-DOS, as can be seen by the light gray shading in Fig. 5. Together with the effect of lifetime broadening of the participating bulk bands it is not surprising that this gap cannot be observed by TCS.

The appearance of two relative band gaps at the zone boundary at $\bar{X}$ will now be used to establish an independent absolute work-function determination of the sample. Symmetry requires the measured band-edge energies to be symmetric as a function of $\mathbf{k}_\parallel$ with respect to $\bar{X}$. If the sample work function is not known, from an experiment it is only possible to determine the angle of incidence θ associated with the point of symmetry. $\mathbf{k}_\parallel$, on the other hand, is determined after Eq. (3) by the preset angle of incidence θ and by the sample work function, since only the kinetic electron energy rather than total energy enters (3). The precision of θ also can be controlled by TCS since, for positive and negative angles of electron incidence, the TCS spectra must be equal. The angular divergence σ_θ of our electron gun is $\approx\pm 2°$ but the focal point of the angular distribution of our gun can be determined with much better precision. However, if a second band edge (either of the same or a different gap) shows up incidentally in the data and it is reasonable to assume that this second edge is also located at the zone boundary, the sets of $E(\theta)$ data can be uniquely converted to $E(\mathbf{k}_\parallel)$ by choosing a sample work function such that both extrema in $E(\mathbf{k}_\parallel)$ show up at the zone boundary because the parallel momentum $\mathbf{k}_\parallel$ at the band edge is well known. The choice of Φ_P influences the symmetry with a sensitivity of 0.1 eV. For Ir(100)-(1×1) our work-function determination employing this symmetry method for all accessible band edges around $\bar{X}$ resulted in $\Phi_{\mathrm{Ir}}^{1\times 1}=6.1\pm 0.1$ eV in perfect agreement with the already cited value of Wandelt.[25]

Within the bulk band region near 12 eV we see another structure with only weak dispersion. This structure is also reproduced qualitatively by the theory but shifted to lower energy values by about 0.4 eV. Near $\bar{\Gamma}$ a structure can be observed at 19.5 eV that has no theoretical counterpart. In this energy region LEED reflections of higher order are possible. A diffraction out of the ΓXUL mirror plane may be responsible for this structure. Also, for the structure within the band gap at $\bar{\Gamma}$ and 7 eV we have no theoretical explanation. The possibility that this structure could be a surface resonance shall be mentioned here but this interpretation must be considered doubtful. The chance to observe effects of the total DOS increases with the number of exchangeable surface lattice vectors and so with the energy of the electrons impinging onto the surface. This will average over a lot of different values of $\mathbf{k}_\parallel$. In addition, surface defects or incommensurable overlayers like the reconstruction will increase diffraction effects out of the selected mirror plane.

The TCS data of the reconstructed (1×5) phase (Fig. 5) show a distinct weakening of the various structures of the (1×1). This is a diffraction effect introduced by the incommensurate first monolayer. This effect can also be observed by other electron-spectroscopic techniques.[29,30] Due to the large surface unit cell of the reconstructed surface, the unit cell in $\mathbf{k}$ space becomes very small. Consequently, the exchangeable reciprocal-lattice vectors and, accordingly, the onset energies for surface umklapp processes, are distinctly smaller than those of the unreconstructed surface. So the gaps around $\bar{X}$ are filled up nearly completely by the large amount of possible diffractions. Even the upper boundary of the gap at 11 eV around $\bar{\Gamma}$ is partially filled by the reconstruction. Also, the structure at 12 eV reduces its intensity and shifts to lower energies. It retains, however, its qualitative dispersion behavior.

The experimental TCS data for the ΓXWK azimuth of Ir(100) are shown in the left part of Fig. 5. The upper boundary of the gap at $\bar{\Gamma}$ and 11 eV is again reproduced well by the theory, but the small bend in the dispersion observed in the experimental data at 0.25 Å^{-1} and 10 eV can hardly be seen in the theory. Similar to the ΓXUL azimuth a structure shows up between 0.2 and 0.8 Å^{-1}. Its mean energy at about 12 eV is expected from theory, but its dispersion shows definite disagreement with expectation.

The big gap around $\bar{M}$ predicted in the energy range from 14 to 21 eV must be shifted to higher energies by about 0.5–1 eV. The qualitative course of the gap boundary is reproduced well by the calculation. A problem exists with the interpretation of the structure in the upper band-gap region around $\bar{M}$, starting at 1.2 Å^{-1} and dispersing downward in the gap. The kinetic energy associated with the parallel momentum $\mathbf{k}_\parallel$ is given by $E(\mathbf{k}_\parallel)=(\hbar^2/2m_c)\mathbf{k}_\parallel^2$. All experimental data presented in Fig. 5 have their origin in states above the vacuum level, even if we reduce the energies by this parallel part $E(\mathbf{k}_\parallel)$. So the assumption of a high-energy bound surface state as an explanation for this structure can be ruled out. A shift of the upper boundary of the bulk gap also gives no solution to this problem because we would then expect an increasing and not a decreasing first derivative in the current as observed. This structure remains, therefore, unexplained.

On the reconstructed (1×5) phase, again, most structures observed on the (1×1) phase are weakened or have even disappeared. The lower boundary of the big gap around $\bar{M}$ seems to be lowered in energy. This structure starts at $|\mathbf{k}_\parallel|=0.85$ Å^{-1} and 18.5 eV and disperses down to the border of the experimentally accessible region at 1.3 Å^{-1} and 15 eV. This structure appears to be a lower boundary of a bulk gap but is located in an energy-versus-momentum region where even an increase in the current should be expected. A similar structure accidentally at the same $\mathbf{k}_\parallel$ can be found in the ΓXUL azimuth. There it crosses $\bar{X}$ and is interrupted at 17 eV by the bulk gap which obviously is filled up only partially. So we may speculate that this structure is connected with the hexagonal first monolayer of the reconstructed phase of Ir(100). Perhaps it is the incompatability of the first layer within the bulk which causes a diffraction out of the mirror plane.

For the (100) surface of platinum in the ΓXUL azimuth we observe similar structures as for iridium (Fig. 6). As discussed before, the work function for the unreconstructed (1×1) phase was determined to be 5.5±0.2 eV

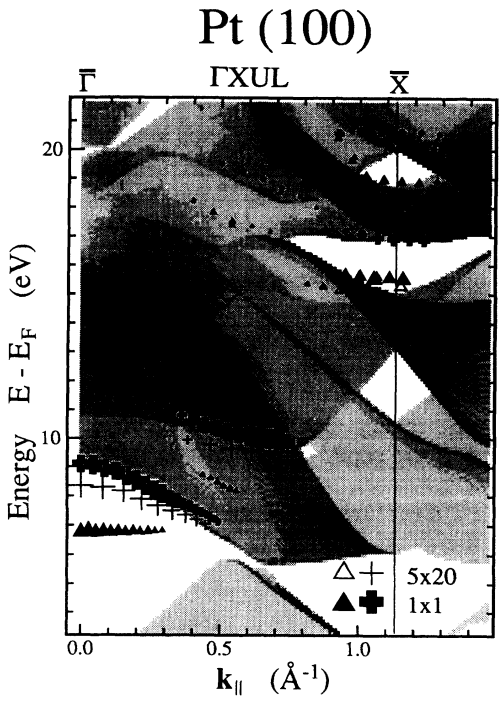

FIG. 6. Maxima and minima of the first derivative TCS data from Pt(100) as a function of $\mathbf{k}_{\parallel}$.

in the same way as for iridium. The difference in the work functions between the (1×1) and the (5×20) modifications is measured by the shift of the onset of the TCS data at the vacuum level to be -0.1 ± 0.05 eV, so the work function of Pt(100)-(5×20) is 5.4 ± 0.2 eV. The symmetry method described above to determine the work function directly is inapplicable to the reconstructed (5×20) phase because the gaps at $\bar{X}$ have vanished.

A view of the bulk gaps of platinum shows that the upper boundary at $\bar{\Gamma}$ and 9 eV is reproduced well by the theory similar to iridium. Also, the gap at $\bar{X}$ and 16 eV and the lower boundary of the gap at 18.8 eV can be explained by the theory. The upper edge of the small gap at 19.5 eV seems to be shifted to energies 1 eV higher than predicted.

The weak-dispersing bulk structure at about 10 eV agrees well with the theory. The agreement here is even better than in the corresponding $E(\mathbf{k}_{\parallel})$ region of Ir(100)-(1×1). The gap at 12 eV around $\bar{X}$ cannot be observed with our experimental geometry because we cannot increase the angle of electron incidence above the value of 66° shown. A main difference between platinum and iridium is found at $\bar{\Gamma}$ and 19.5 eV: The strong current rise for iridium can hardly be detected on the platinum sample.

The reconstruction geometry of Pt(100) is very similar to that of Ir(100).[31,32] Pt(100) also forms a quasihexagonal first monolayer. This surface modification again partially fills the gap at $\bar{\Gamma}$. The upper boundary of this gap shifts downward to 8.2 eV. The flat structure near 10 eV also shifts downward by 0.8 eV as observed on iridium. Both gaps around $\bar{X}$ have vanished nearly completely.

SUMMARY

We have shown that TCS is a sensitive tool for testing some aspects of bulk-band-structure calculations in the region above the vacuum level. In addition, the technique is simple to handle experimentally if an electron gun is available with emission characteristic exhibiting only weak current variations over the required energy range. We have presented a way to calculate a one-dimensional "nearly-free-electron DOS." Extrema in the first derivative of our experimental TCS data are compared to the NFE-DOS. This explains most of the observed current structures. If two or more bulk gaps at the zone boundaries are accessible by TCS, a method for absolute work-function determination is obtained. Our independent data for the work function for the unreconstructed phases of Ir(100) and Pt(100) are $\Phi=6.1\pm0.1$ and 5.5 ± 0.2 eV, respectively. Decreases in the work function caused by surface reconstruction can be seen by the shift of the onset of the TCS spectra. These decreases are $\Delta\Phi=0.2\pm0.05$ eV for iridium and $\Delta\Phi=0.1\pm0.05$ eV for platinum. Finally, we have shown that reconstruction of a surface partially fills up symmetry gaps and bulk band gaps.

ACKNOWLEDGMENT

We would like to thank M.-L. Hirschinger for her valuable help with the measurements.

[1]J. B. Pendry, *Low Energy Electron Diffraction* (Academic, London, 1974).
[2]J. Rundgren and G. Malmström, J. Phys. C **10**, 4671 (1977).
[3]G. Malmström and J. Rundgren, Comput. Phys. Commun. **19**, 263 (1980).
[4]R. O. Jones and P. J. Jennings, Surf. Sci. Rep. **9**, 165 (1988).
[5]M. Lindroos, H. Pfnür, and D. Menzel, Phys. Rev. B **33**, 6684 (1986).
[6]R. C. Jaclevic and L. C. Davis, Phys. Rev. B **26**, 5391 (1982).
[7]E. Tamura, R. Feder, J. Krewer, R. E. Kirby, E. Kisker, E. L. Garwin, and F. K. King, Solid State Commun. **55**, 543 (1985).
[8]K. G. McKay, *Advances in Electronics and Electron Physics I* (Academic, New York, 1948).
[9]E. M. Baroody, Phys. Rev. **78**, 780 (1950).
[10]H. Bruining, *Physics and Applications of Secondary Electron Emission* (Pergamon, London, 1954).
[11]A. J. Dekker, Solid State Phys. **6**, 251 (1958).
[12]I. Schäfer, M. Schlüter, and M. Skibowski, Phys. Rev. B **35**, 7663 (1987).
[13]V. Dose, Th. Fauster, and R. Schneider, Appl. Phys. **40**, 202 (1986).
[14]R. Schneider, H. Dürr, Th. Fauster, and V. Dose, J. Vac. Sci. Technol. A **8**, 3363 (1990).
[15]J. Hölzl and F. K. Schulte, in *Solid Surface Physics*, edited by G. Höhler (Springer, Berlin, 1979), p. 45.
[16]J. Noffke and L. Fritsche, J. Phys. F **12**, 921 (1982).
[17]G. Leschik, R. Courths, H. Wern, S. Hüfner, H. Eckardt, and J. Noffke, Solid State Commun. **52**, 221 (1984).

[18]M. T. Johnson, A. R. Law, and H. P. Hughes, Surf. Sci. **162**, 11 (1985).
[19]J. B. Pendry, in *Photoemission and the Electronic Properties of Surfaces,* edited by B. Feuerbacher, B. Fitton, and R. F. Willis (Wiley, New York, 1978), p. 96.
[20]W. Altmann, Dissertation thesis, University of Würzburg, 1988.
[21]V. Dose, Th. Fauster, and R. Schneider, Appl. Phys. A **40**, 203 (1986).
[22]J. T. Grant, Surf. Sci. **18**, 228 (1969).
[23]M. A. van Hove, R. J. Koestner, P. C. Stair, J. P. Biberian, L. L. Kesmodel, I. Bartos, and G. A. Somorjai, Surf. Sci. **103**, 218 (1981).
[24]T. N. Rhodin and G. Broden, Surf. Sci. **60**, 466 (1976).
[25]K. Wandelt, J. Vac. Sci. Technol. A **2**, 802 (1984).
[26]J. Küppers and H. Michel, Appl. Surf. Sci. **3**, 179 (1979).
[27]R. Courths, H.-G. Zimmer, A. Goldmann, and H. Saalfeld, Phys. Rev. B **34**, 3577 (1986).
[28]N. Müller, B. Kessler, B. Schmiedeskamp, G. Schönhense, and U. Heinzmann, Solid State Commun. **61**, 187 (1987).
[29]J. F. van der Veen, F. J. Himpsel, and D. E. Eastman, Phys. Rev. B **22**, 4226 (1980).
[30]R. Drube, V. Dose, and A. Goldmann, Surf. Sci. **197**, 317 (1988).
[31]P. Heilmann, K. Heinz, and K. Müller, Surf. Sci. **83**, 487 (1979).
[32]K. Heinz, E. Lang, K. Strauss, and K. Müller, Surf. Sci. **120**, L401 (1982).

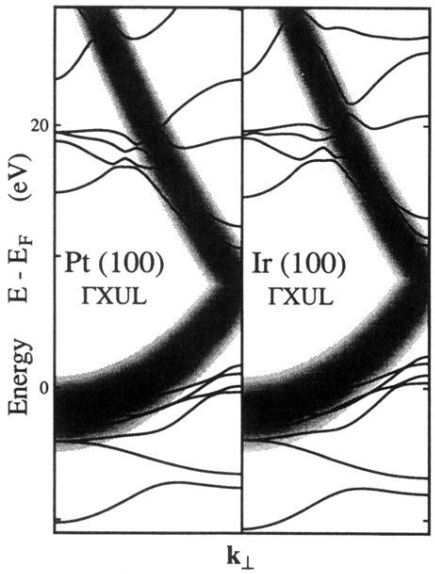

FIG. 2. Comparison of the bulk band structure of iridium and platinum for normal electron incidence with the free-electron parabola lowered by the inner potential of 2 eV. The broadening of the parabola shall quantify the lifetime broadening of the excited states and shows the range of acceptance for free-electron-like bulk bands.

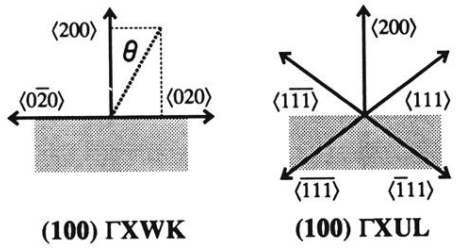

FIG. 3. The smallest reciprocal-lattice vectors of the (100) surface in the ΓXUL and the ΓXWK azimuth. The gray box symbolizes the bulk region.

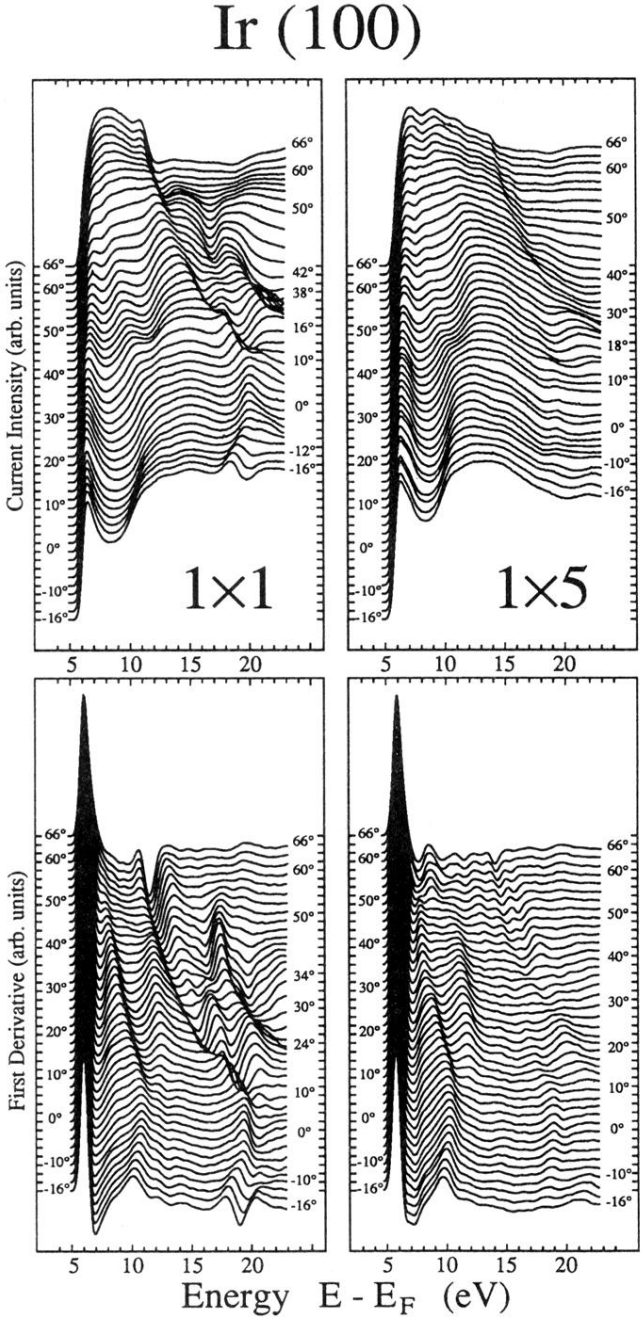

FIG. 4. Target current spectra from the unreconstructed 1×1 and the reconstructed 1×5 surface modification of Ir(100) in the ΓXUL azimuth. For both modifications the original data and their first derivatives are presented.

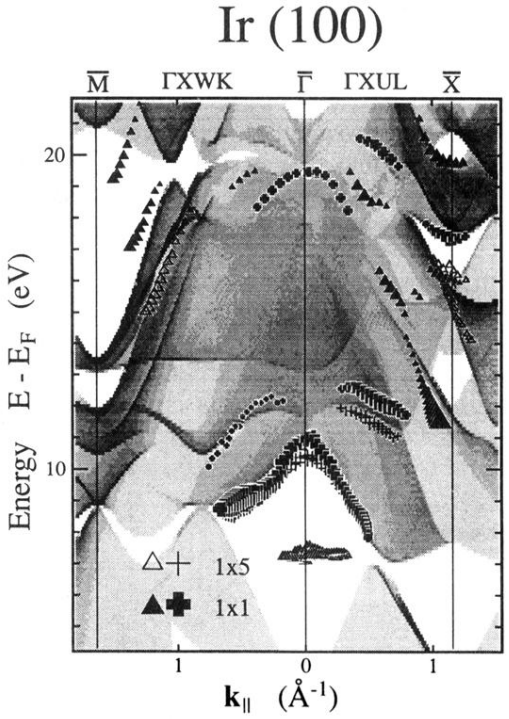

FIG. 5. Maxima and minima of the first derivative TCS data from Ir(100) in the ΓXUL (right part) and the ΓXWK azimuth (left part) as a function of $\mathbf{k}_{\|}$. With a linear gray scaling the NFE-DOS $(E,\mathbf{k}_{\|})$ of the surfaces are symbolized.

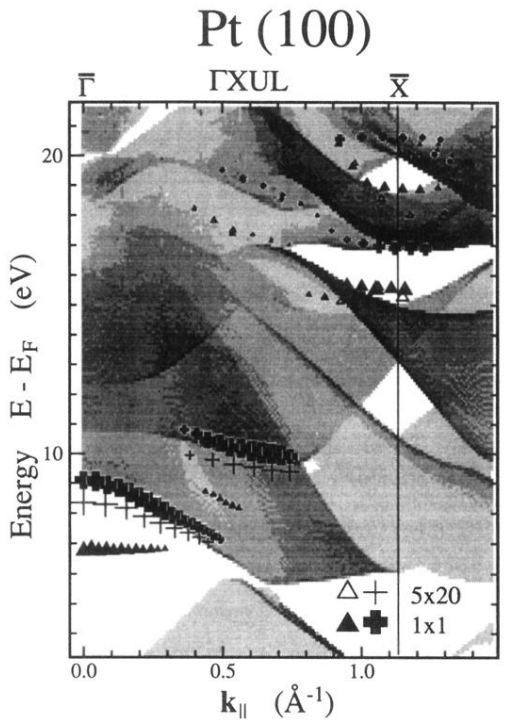

FIG. 6. Maxima and minima of the first derivative TCS data from Pt(100) as a function of $\mathbf{k}_{\parallel}$.